



**HAL**  
open science

## Interplay between core, edge and scrape-off layer in turbulent magnetised plasmas

Guilhem Dif-Pradalier, Ph. Ghendrih, Y. Sarazin, X. Garbet, V Grandgirard, Y. Munsch, R. Varennes, L. Vermare, Y. Camenen, F. Widmer

### ► To cite this version:

Guilhem Dif-Pradalier, Ph. Ghendrih, Y. Sarazin, X. Garbet, V Grandgirard, et al.. Interplay between core, edge and scrape-off layer in turbulent magnetised plasmas: Lessons learnt from an information theoretic measure, the "transfer entropy" to assess causality in nonlinear plasma dynamics. FEC 2020 - IAEA Fusion Energy Conference, May 2021, E-Conference, France. cea-03287143

**HAL Id: cea-03287143**

**<https://cea.hal.science/cea-03287143>**

Submitted on 15 Jul 2021

**HAL** is a multi-disciplinary open access archive for the deposit and dissemination of scientific research documents, whether they are published or not. The documents may come from teaching and research institutions in France or abroad, or from public or private research centers.

L'archive ouverte pluridisciplinaire **HAL**, est destinée au dépôt et à la diffusion de documents scientifiques de niveau recherche, publiés ou non, émanant des établissements d'enseignement et de recherche français ou étrangers, des laboratoires publics ou privés.

# INTERPLAY BETWEEN CORE, EDGE AND SCRAPE-OFF LAYER IN TURBULENT MAGNETISED PLASMAS

*Lessons learnt from an information theoretic measure, the “Transfer Entropy” to assess causality in nonlinear plasma dynamics.*

G. Dif-Pradalier<sup>1</sup>, Ph. Ghendrih<sup>1</sup>, Y. Sarazin<sup>1</sup>, X. Garbet<sup>1</sup>, V. Grandgirard<sup>1</sup>, Y. Munschy<sup>1</sup>, R. Varennes<sup>1</sup>, L. Vermare<sup>2</sup>, Y. Camenen<sup>3</sup>, F. Widmer<sup>3</sup>

- 1) CEA, IRFM, F-13108 Saint-Paul-lez-Durance cedex, France.
- 2) L.P.P. Ecole Polytechnique, Palaiseau, France.
- 3) CNRS, Aix-Marseille Univ., PIIM UMR7345, Marseille, France.

Email: guilhem.dif-pradalier@cea.fr

## Abstract

The present manuscript is meant to provide a companion pedagogical approach to an information theoretic measure, the “Transfer Entropy” method, useful to assess causality in complex (time series) datasets. This manuscript describes useful basics for the forthcoming discussion on the causal chain of events that leads to the onset of a spontaneous and stable edge transport barrier in flux-driven gyrokinetics when core, edge and scrape-off layer regions self-consistently interplay.

## 1. INTRODUCTION

For over three decades, the observation of rapid core confinement improvement upon favourable modifications of edge operating conditions has been a nagging source of puzzlement for experimentalists investigating conditions for a lasting source of fusion energy in tokamaks. The transport properties of drift-wave turbulence and the interaction of the confined plasma with its material boundaries have long been recognised as essential to the resolution of this conundrum. Key aspects of the turbulent dynamics in the plasma edge are poorly quantified, owing to the disparity of temporal and spatial scales and the inadequacy of performing scale separations. A forthcoming paper [1] will be detailing three key results that arise when a material boundary is introduced in flux-driven gyrokinetics, effectively interconnecting core, edge and Scrape-Off Layer (SOL) regions. We show that (a) turbulence is not only locally driven by local gradients but nonlocally controlled by fluxes of turbulence activity, primarily though not exclusively borne at the edge. This ‘nonlocal’ influence is mediated through vortex-flow localised interactions near the material boundaries and has two major consequences: (b) the nonlinear destabilisation of the linearly stable edge, providing a possible resolution for the so-called ‘shortfall’ conundrum and (c) the spontaneous emergence of a stable and localised transport barrier at the closed/open field line transition, possible prelude to the formation of a pedestal. In the present manuscript, we focus on the latter point and discuss a general technique, the so-called “Transfer Entropy” imported from information theory that provides a useful tool to assess the causal chain of events that leads to the onset of this stable edge transport barrier. This point is of course of basic interest: it allows to precisely test theoretical frameworks from the perspective of primitive equations and as such provides important guidelines for reduced modelling.

## 2. CHAIN OF CAUSALITY AND THE “TRANSFER ENTROPY” (T.E.) METHOD

Unravelling causal chains of events in complex datasets is challenging yet especially rewarding when the dataset stems from either experimental measurements or has been computed from the primitive equations. Low-frequency microturbulence in fusion plasmas is appropriately described by gyrokinetics. GYSELA[2] models ions and trapped electrons gyro-kinetically in the core and edge regions as well as the closed/open field line transition and the Scrape-Off Layer (SOL) through introduction of a simplified penalised limiter[3] mimicking the role of a heat and momentum sink. Core, edge and SOL are treated on an equal footing. As we find strong interplay between these distinct regions and the spontaneous development of a stable edge transport barrier, the flux of information across the edge is complex and typically not merely locally influenced. In other words, its evolution is not only subject to variations of the local free energy, ie. the mean local gradients. Investigating techniques that may allow to disentangle the causal chain of events is very desirable and would provide quantitative insight regarding the dominant feedback loops involved.

Causality detection in information theory is actively debated [4]. We will focus here on a simple nonlinear extension of the Granger causality, introduced by Schreiber [5] as the "Transfer Entropy" (TE) method and investigated in magnetised plasmas by Van Milligen et al. [6] and Nicolau [7]. Let us state at this point that our goal here is not to provide a discussion on the concept of causality itself but rather put to use one of its possible manifestations –defining causality let alone inferring it is indeed still lively discussed [8]. The idea behind TE is simple yet powerful: let's consider a time series  $(x_i)$  with  $0 \leq i \leq n$ , of realisations of observable X. If one can better predict its next realisation  $x_{n+1}$  using additional data from another time series  $(y_j)$  with  $0 \leq j \leq n$  of observable Y, then we shall say that "Y transfers information (i.e. causes) X", or more accurately as "Y forecasts X", which constitutes our definition of causality here. This idea is quantified measuring deviation of transition probabilities from independence, i.e. from a stationary Markov process. In its simplest expression, as used here, if processes X and Y are independent, then the following generalised Markov property holds for all  $0 \leq k \leq n$ :  $p(x_{n+1}|x_{n-k}, y_{n-k}) = p(x_{n+1}|x_{n-k})$ . The standard notation for conditional probabilities is used here:  $p(a|b)$  is the probability of a knowing b. If now processes X and Y are not independent, the ratio of these two transition probabilities provides a measure of how much information they may share, i.e. how much knowing values in Y in addition to past values in X may help to better evaluate next-step  $x_{n+1}$ . This idea leads to the following definition of the Transfer Entropy (TE) from process Y to process X:

$$TE_{Y \rightarrow X}(k) = \sum p(x_{n+1}, x_{n-k}, y_{n-k}) \log \left( \frac{p(x_{n+1}|x_{n-k}, y_{n-k})}{p(x_{n+1}|x_{n-k})} \right) \quad (1)$$

where k is thus a time lag and represents the k-past of times series X and Y. The summation process is detailed below, in Eq.(3). The TE can equivalently be recast as a conditional mutual information and represents the additional amount of information that must be added to adequately represent the studied process  $p(x_{n+1}|x_{n-k}, y_{n-k})$  with respect to its reference Markov process  $p(x_{n+1}|x_{n-k})$ . In the absence of information flow from Y to X, the logarithm vanishes as the state of Y has no influence on the transition probabilities of X –another way of saying that Eq.(1) indeed quantifies a "transfer" of information. It also follows that TE is directional, i.e.  $TE_{Y \rightarrow X} \neq TE_{X \rightarrow Y}$ , which allows to infer causality between processes X and Y. It is also to be noted that TE is quite generic and displays interesting properties: it is independent of the relative magnitudes of signals X and Y; it may apply to either linear and nonlinear regimes; it is easy to evaluate (directly in real space rather than in Fourier space) and typically less demanding in terms of statistics than bispectral techniques.

Practically, TE is evaluated expressing the conditional probabilities as joint probabilities, eg.  $p(x_{n+1}|x_{n-k}, y_{n-k}) = p(x_{n+1}, x_{n-k}, y_{n-k})/p(x_{n-k}, y_{n-k})$  and computing the 4 multidimensional probability density functions (pdfs):

$$TE_{Y \rightarrow X, \alpha}(k) = \sum p^\alpha(x_{n+1}, x_{n-k}, y_{n-k}) \log^\alpha \left( \frac{p(x_{n+1}, x_{n-k}, y_{n-k}) p(x_{n-k})}{p(x_{n+1}, x_{n-k}) p(x_{n-k}, y_{n-k})} \right) \quad (2)$$

as a function of time delay k and normalised such that  $0 \leq TE \leq 1$ . The 4 pdfs in Eq.(2) result from a binning process of times series X and Y, such that Eq.(2) is estimated in practice as:

$$TE_{Y \rightarrow X, \alpha}(k) = \sum_{i=1}^{\beta} \sum_{j=1}^{\beta} \sum_{l=1}^{\beta} [p^{3d}(i, j, l)]^\alpha \log^\alpha \left( \frac{p^{3d}(i, j, l) p^{1d}(j)}{p_{xx}^{2d}(i, j) p_{xy}^{2d}(j, l)} \right) \quad (3)$$

where  $p^{3d}$ ,  $p^{2d}_{xx}$ ,  $p^{2d}_{xy}$  and  $p^{1d}$  are the discretised versions of respectively  $p(x_{n+1}, x_{n-k}, y_{n-k})$ ,  $p(x_{n+1}, x_{n-k})$ ,  $p(x_{n-k}, y_{n-k})$  and  $p(x_{n-k})$ . In order to have sufficient statistics, the bin size "β" is typically chosen as  $\beta=2$  or  $\beta=3$ , depending on the available length of the time series (the longer the times series, the larger β can be). Eq.(3) now clarifies the way to perform the summation in Eqs.(1) and (2).

Here we have also introduced the additional exponent  $\alpha \geq 1$ , which effectively represents a nonlinear threshold: low probabilities will be further reduced and higher ones amplified. In the following, we take  $\alpha=1$ . In a complex setting, information may flow both ways, from Y to X and inversely. It is thus especially useful to define the net transfer entropy  $\Delta_{X,Y}(TE)[k] = TE_{Y \rightarrow X}[k] - TE_{X \rightarrow Y}[k]$ , which provides the net flow of information between processes X and Y, at timelag k. This is the quantity that we now discuss in further detail.

### 3. MANUFACTURED SOLUTIONS AND PROOF OF CONCEPT

TE is found to be weakly dependent on a few choices that the user must perform: in the following, we discretise the pdf in Eq.(2) using  $\beta^d=2^d$  bins, with d the dimensionality of the pdf. The magnification exponent  $\alpha$  is set to unity and X and Y are discretised at the same rate and chosen to enter the TE calculation with zero temporal mean. In order to provide a pedagogical introduction to the interpretation of transfer entropy graphs, let us detail the following manufactured solutions. In Fig.1 we show the example for a random time series X. Y is

constructed such that it exactly corresponds to X, with a forward in time delay of 9 units. As only past information may be shared between X and Y and as time lag k tests for similarities in shape of processes X and Y,  $TE(Y \rightarrow X)$  should be vanishing for all time lags for a random time series and display a marked peak around time lag  $k=9$  for the  $TE(X \rightarrow Y)$ . The net TE simply states that for all the 50 time lags considered here, the only meaningful flow of information can go from  $X \rightarrow Y$ , with a time lag of 9.

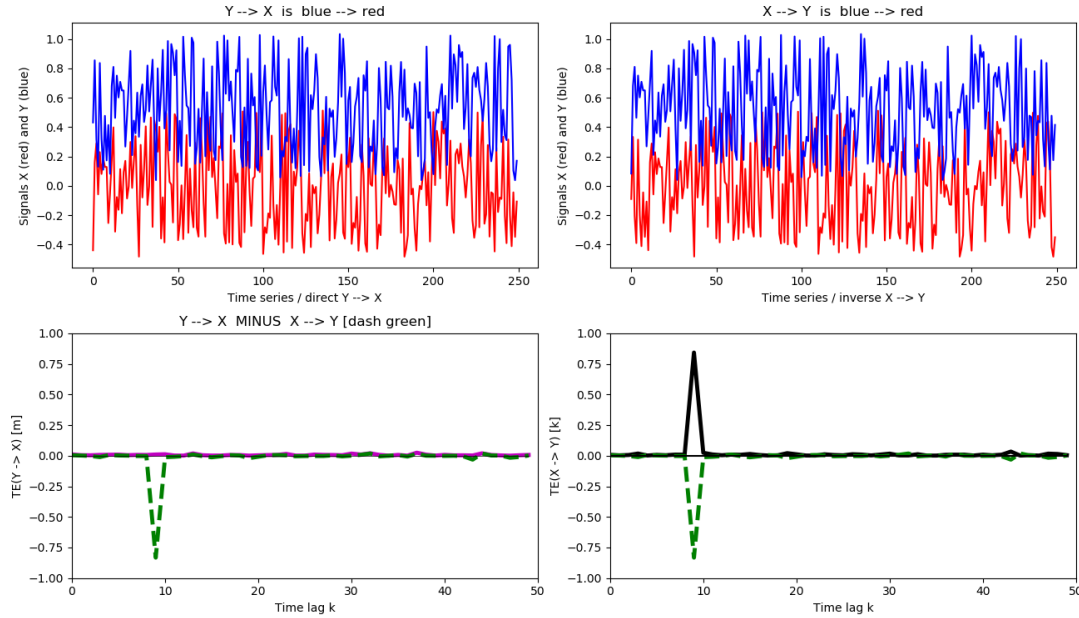


Figure 1. (Top left and right) Time traces of the two processes X and Y over which TE is computed. For visualisation purposes only, Y is offset by its maximum value.  $TE(Y \rightarrow X)$  is represented (lower left) in purple and  $TE(X \rightarrow Y)$  in black (lower right) as a function of time lag k. The net Transfer Entropy  $\Delta_{X,Y}(TE)$  is displayed as well (dashed green).

Similarly, in Fig.2, focussing on the left panel, the blue peak at time=31 from process Y may transfer information to the two peaks of process X at times=40 and 140, the former with a time lag=9, the latter with a time lag=109. Inversely, considering the reverse  $TE(X \rightarrow Y)$ , the peak at time=40 may only transfer information towards peaks at time=69, 131, and 169 and not to the previous in time=31 peak.

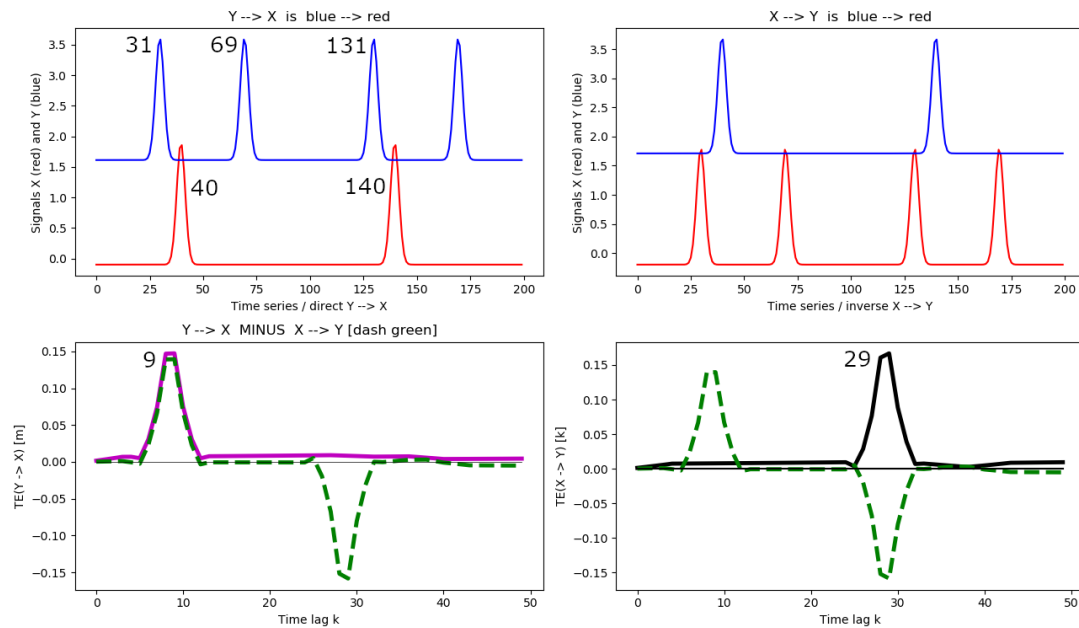


Figure 2. Time traces of processes X and Y and associated TE calculations; colour coding and legends are as in Fig.1.

This illustrates causality in the flow of time and clarifies the reason of  $TE(X \rightarrow Y)$  peaking at time lags = 29, 91, ... (bottom right panel). It also shows that the TE technique does not require many occurrences of causal events to unambiguously extract relevant flows of information.

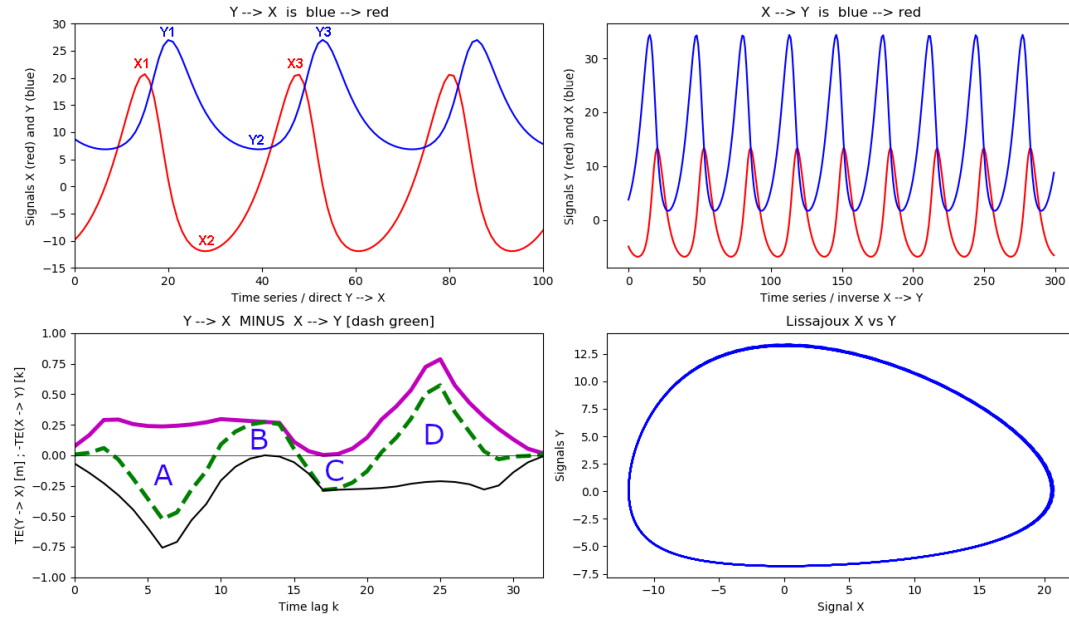


Figure 3. TE applied to the Lotka-Volterra equations; colour coding and legends are as in Fig.1.

Another typical situation, common in nonlinear dynamics is illustrated in Fig.3, simulating predator-prey behaviour from the Lotka-Volterra equations:

$$\frac{du}{dt} = au - buv \quad (4)$$

$$\frac{dv}{dt} = cuv - dv \quad (5)$$

with parameters  $a = 1$ ,  $b = 0.1$ ,  $c = 0.075$  and  $d = 1.5$ . The typical cyclic behaviour between predator and prey is readily seen through the Lissajoux display (bottom right panel) of process  $X$  (the prey) as a function of the predator  $Y$ . Where correlation analysis would merely pick up the periodicity of the predator and prey oscillations, this example illustrates the usefulness of the net Transfer Entropy  $\Delta_{X,Y}(TE)$  (dashed green, lower left panel) as it provides guidance regarding the flow of information, as the nonlinear system evolves. Individual TE curves provide knowledge on typical waiting times for the system to reach a given state. For instance,  $TE(X \rightarrow Y)$  [black, lower panel] tells us that starting from a large number of preys ( $X1$ ), the system will need about  $k \sim 6$  time steps to reach a state with a large number of predators ( $Y1$ ). Inversely, from  $TE(Y \rightarrow X)$  starting from a large predator state ( $Y1$ ), the system will require  $k \sim 25$  time lags to be able to sustain again a large number of preys ( $X3$ ). Of course, in a complex system information keeps flowing between preys and predators during the whole oscillation period. Net TE  $\Delta_{X,Y}(TE)$  captures inflexion points relevant for the dynamics. Thus, peak A corresponds to the situation where an increase in prey numbers or a large abundance of preys triggers a large predator growth with time lag  $\sim 6$ . In stage B, predators in large numbers now eat more preys than their birthrate manages to compensate and decimates their numbers. During stage C, preys in fewer numbers trigger a decline in predator numbers with a time lag  $\sim 18$ . The low predator population in stage D now triggers with a time lag  $\sim 25$  the increase in prey growth and the system loops again.

#### 4. T.E. APPLIED TO THE FAR-EDGE REGION WHERE A TRANSPORT BARRIER DEVELOPS

We now systematically compute the TE algorithm to actual time series from large-scale GYSELA flux-driven computations with limiter boundary conditions in the last 5% inside the last closed flux surface (LCFS) where the spontaneous onset of a persistent transport barrier is observed. A vorticity equation [9] can be inferred from

the primitive gyrokinetic equations including  $\mathbf{ExB}$  drift and finite Larmor radius effects and can be recast at leading order as follows:

$$\partial_t \langle \Omega_r \rangle + \frac{1}{r} \partial_r r \left[ \langle v_{Er} \Omega_r \rangle + \langle v_{\star r} \Omega_r \rangle - \left\langle v_{\star \theta} \frac{1}{r} \partial_\theta E_r \right\rangle \right] = r.h.s \quad (6)$$

$$r.h.s \approx -\partial_t \langle \Omega_\theta \rangle - \frac{1}{r} \partial_\theta \langle (v_{E\theta} + v_{\star \theta}) \Omega_\theta \rangle - \partial_r \frac{1}{2r} \partial_\theta \langle v_{E\theta}^2 \rangle + \frac{1}{2r^3} \partial_\theta \partial_r \langle r^2 v_{Er}^2 \rangle - \frac{1}{r} \partial_\theta \left\langle v_{\star r} \frac{1}{r} \partial_\theta v_{E\theta} \right\rangle \quad (7)$$

$$\Omega_r = \partial_r (r \partial_r \phi) / r \quad \& \quad \Omega_\theta = \partial_\theta^2 \phi / r^2 \quad (8)$$

$$v_{Er} = -\partial_\theta \phi / r \quad \& \quad v_{E\theta} = \partial_r \phi = -E_r \quad (9)$$

$$v_{\star r} = -\partial_\theta p_\perp / r \quad \& \quad v_{\star \theta} = \partial_r p_\perp \quad (10)$$

with  $r$  and  $\theta$  respectively the minor radius and poloidal angle and  $\langle \bullet \rangle$  denoting an average over toroidal angle  $\varphi$ . We have applied the TE algorithm to many of the possible permutations of quantities in Eq.(6) and especially to the following set:

$$(X, Y) \in \left\{ \langle \Omega_r \rangle, \langle v_{Er} \Omega_r \rangle, \langle v_{\star r} \Omega_r \rangle, - \left\langle v_{\star \theta} \frac{1}{r} \partial_\theta E_r \right\rangle, \dots \right\} \quad (11)$$

We focus here on the example where 'X' is the vorticity and 'Y' a "field advection" [first and fourth terms in the bracket of Eq.(11)]. This latter term is somewhat uncommon; physically it corresponds to a poloidal advection by diamagnetic currents of poloidal anisotropies of the radial electric field  $E_r$ . Each field is radially and poloidally averaged respectively over the last 5% of the plasma volume and  $\pi/3$  region symmetric about the limiter. The net transfer entropy  $\Delta_{X,Y}(TE)$  between vorticity and poloidal tilt is displayed in Fig.4. For two periodic fields, the investigated time lag should have an upper bound which, as can be intuitively understood from Figs.2 and 3 is the shortest of the two fields' periods. Here, none of X or Y are strictly periodic; the upper bound  $k_{max}$  for time lag  $k$  is chosen as the shortest "period" that is inferred from the dominant Fourier mode in each field. Upper bound  $k_{max}$  could also be inferred [6] from a time-delayed self-mutual information; both methods render comparable estimations:  $k_{max} \sim 4000 \Omega_{ci}$ , with  $\Omega_{ci}$  denoting the ion cyclotron frequency. Let us also introduce  $A_{>0} = \int_0^{k_{max}} \max[0, \Delta_{X,Y}(TE)] dk$  and  $A_{<0} = \int_0^{k_{max}} \min[0, \Delta_{X,Y}(TE)] dk$  the areas of respectively positive (yellow area, Fig.4, centre) and negative net TE (purple area, same figure).

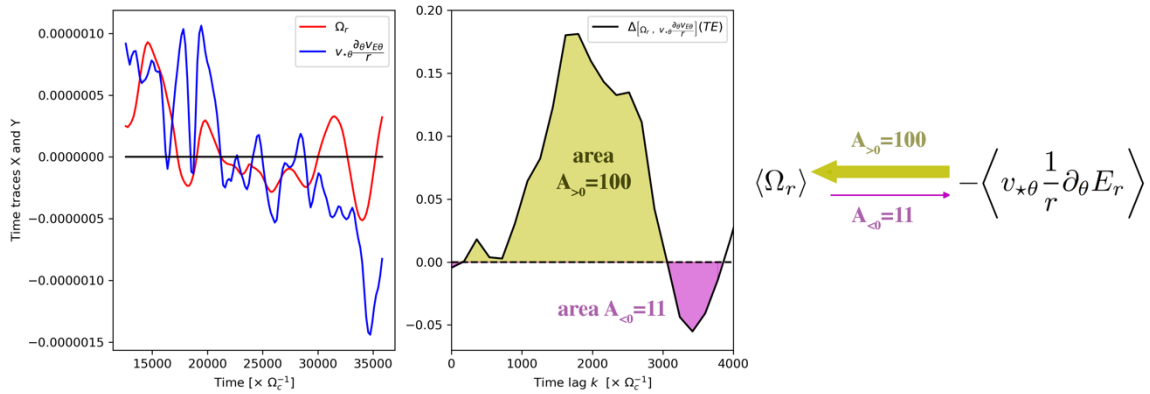


Figure 4. Causality, as inferred from the application of the TE algorithm to the actual time series of vorticity and poloidal tilt (left panel), from flux-driven gyrokinetic computations near the LCFS, at inception of an edge transport barrier. The net TE is show in the central panel, the net flow of information reversing between positive and negative areas. The arrows on the right panel are a convenient way to synthetise this data, their direction indicating the flow of information and their width (resp. 100 vs 11) the amount of information actually transferred between both quantities.

As detailed above, net TE  $\Delta_{X,Y}(TE)$  provides a quantitative measure of the direction and intensity of information flow. These facts are conveniently summarised diagrammatically (right panel of Fig.4): (i) the *direction* of information flow (direction of the arrow) is given by  $\Delta_{X,Y}(TE)$ , either positive or negative whilst (ii)  $A_{>0}$  [resp.  $A_{<0}$ ] is a proxy for the *amount* of information transferred from  $Y \rightarrow X$  [resp.  $X \rightarrow Y$ ] during one "period". In the

example displayed in Fig.4,  $A_{>0}/A_{<0} \approx 100/11$ ; the thickness of each arrow relative to the next in the diagrammatic representation is set to follow the same ratio so that respective thickness and direction of connecting arrows provide a visual representation of causality and amount of information actually transferred between considered fields.

This analysis has been systematically performed, for all combination of terms in Eqs.(6)-(10). Unexpectedly, the diamagnetic advection of vorticity [2<sup>nd</sup> term in the bracket of Eq.(6)] also appears as a key contributor to vorticity build-up in the early onset of the edge transport barrier. These facts certainly point towards an important role for diamagnetic currents, i.e. poloidal distribution of pressure fluctuations that stem from spontaneous symmetry breaking induced through plasma—boundary interplay. These results are discussed in a forthcoming paper.

## 5. CONCLUSIONS AND OUTLOOK

The present manuscript has focused on laying out useful basics to assess causality in time series analysis, through the use of the so-called “Transfer Entropy” method, a nonlinear extension of the Granger causality. Practical use of this method, applied to the nonlinear onset of an edge transport barrier in advanced gyrokinetic computations of tokamak turbulence will be reported shortly elsewhere [1].

## ACKNOWLEDGEMENTS

The authors want to thank Ch. Passeron for continued help with the development of GYSELA and acknowledge stimulating discussions with P.H. Diamond and participants at the 2019 Festival de Théorie in Aix-en-Provence. The work has been carried out within the framework of the EUROfusion Consortium and was supported by the EUROfusion Theory and Advanced Simulation Coordination (E-TASC) initiative under the TSVV (Theory, Simulation, Verification and Validation) “L-H transition and pedestal physics” project (2019-2020). It has also received funding from the Euratom research and training program. The project has received funding from the European Union Horizon 2020 research and innovation program under grant agreement No 824158 (EoCoE-II). The views and opinions expressed herein do not necessarily reflect those of the European Commission. This work was also granted access to the HPC resources of TGCC and CINES made by GENCI, and to the EUROfusion High Performance Computer Marconi-Fusion. We acknowledge PRACE for awarding us access to Joliot-Curie at GENCI@CEA, France and MareNostrum at Barcelona Supercomputing Center (BSC), Spain.

## REFERENCES

- [1] G. Dif-Pradalier, et al., to be submitted (2021).
- [2] V. Grandgirard, et al. *Computer Physics Communications*, 207:35, 2016
- [3] E. Caschera, et al. *Journal of Physics: Conf. Series* 1125:012006, 2018
- [4] K. Hlavackova, et al. *Physics Reports* 441(1):1, 2007
- [5] T. Schreiber, *Phys. Rev. Letters* 85:461, 2000
- [6] B.Ph. van Milligen, et al. *Nucl. Fusion* 54:023011, 2014
- [7] J.H. Nicolau, et al. *Phys. Plasmas* 25:102304, 2018
- [8] C.W.J. Granger, *J. Econ. Dynam. Control* 2:329, 1980
- [9] Y. Sarazin, et al. *Plasma Phys. Contr. Fusion*, 103275.R2, 2021